The Influence of Chromatic Components on Extended Depth of Field Imaging

JAVIER NAVAS* AND JOAQUÍN MARTÍN
Physical Chemistry Department, Science Faculty, University of Cadiz, Pol. Río San Pedro s/n. 11510 Puerto Real Cádiz, Spain

KEY WORDS extended depth of field; focusing; chromatic components; image processing

ABSTRACT The analysis of variance is one of the most commonly used algorithms for detecting focalized zones in digital images and is an entry point to extended focalization techniques beyond those established by optical laws. This article analyses the dependence of the red, green, and blue (RGB) and lightness, hue, and saturation (LHS) components when used as the basis for applying an algorithm to obtain images with extended depth of field. Also, an algorithm developed by the authors is described and the dependence of the final result is shown according to the chromatic components used as the variables. Finally, a methodology is defined based on the study of second variance in relation to the number of images and pixels of the chromatic coordinates to decide which to use as the basis for the calculation. *Microsc. Res. Tech. 72:403–410, 2009.*

INTRODUCTION

Solving the problem of depth of field limitations when using high magnification lenses is of great interest in fields such as Medicine or Biomedicine (Amar et al., 2008; Chen et al., 2008; Iliev and Wouters, 2007; Mironova et al., 2007; Scalfi-Happ et al., 2007), Biology (Heisterkamp et al., 2007; Scrimgeour et al., 2007; Zhang et al., 2007) or Material Science (Hashimoto et al., 2007; Nair et al., 2008; Snyder et al., 2007; Wickramasinghe et al., 2006). Different techniques have been proposed in the recent years to obtain images with an extended depth of field, which is the range of distance in front of and behind an object focused by an optical instrument within which other objects will also appear clear and sharply defined in the resulting image. This is a particularly relevant magnitude in optical microscopy, especially when working at high magnification, due to its small value in the visible spectral range. Basically, the previously proposed methods can be placed into two groups: (a) those that improve the optical parameters of the instrumentation and (b) those that, through the use of mathematical algorithms applied to a stack of digital images, are able to detect the focalized sectors of each image, which are then merged to construct an image with an extended depth of field.

Normally, optical methods are based on the improvement of the optical transfer function (OTF) of the defocused system (Widjanarko and Hardie, 2002), increasing the optical response at high spatial frequencies. McCrikerd (1971) has shown that it is possible to use an annular aperture to extend the spatial frequency response of the modulation transfer function (MTF). These methods provide on-line improvements, but involve extra work and the use of expensive, new components in the optical system used.

Using the other approach, Sugimoto and Ichioka (1985) show that better results are obtained using algorithms to treat the images (in this case an algorithm based on the study of local variance) rather than using optical methods to improve the OTF. These methods do not generate instantaneous results, but do offer greater flexibility and do not require the microscope's optical elements to be modified. The common working basis of these methods can be summarized in three steps: (a) obtaining a set of images of the object with different lens-object distances, either in an automated or manual way, (b) mathematical treatment of the images obtained to detect and extract the focalized sectors, and (c) merging the focalized sectors and generating an image with an extended depth of field.

The algorithms that these methods use are based on the maximization of a function from which it is possible to detect the focalized sectors. For example, Widjanarko and Hardie (2002) use the Fourier transform as a function. Burt and Lolzcynski (1993) proposed a method based on variance and the use of a wavelet transform. Li et al. (1995) propose a method in which a wavelet maximal function is used as the selection criteria. Valdecasas et al. (2001) use a method that is basically a hybrid of Burt and Lolzcynski's and Li et al.'s methods. Itoh et al. (1989) developed two algorithms, one based on the measurement of local variance and the other based on the nondirectional difference operator. González and Woods (1992) and Castleman (1996) use the Sobel Operator, which is an edge detector with some noise smoothing incorporated that returns a measure of the strength of an edge being present at a given pixel. Sugimoto and Ichioka (1985) developed an algorithm which is also based on the study of local variance. Pieper and Korpel (1983) developed three algorithms by studying the intensity of each pixel (the

*Correspondence to: Javier Navas; Physical Chemistry Department, Science Faculty, University of Cadiz, Pol. Río San Pedro s/n. 11510 Puerto Real Cádiz, Spain. E-mail: javier.navas@uca.es

Received 26 September 2008; accepted in revised form 6 December 2008

DOI 10.1002/jemt.20685

Published online 22 January 2009 in Wiley InterScience (www.interscience.wiley.com).

focal point will coincide with a maximum or minimum intensity value), the variance and a nondirectional difference operator. The use of variance is a recurrent resource for resolving the problem of distance detection in autofocus systems. Some of the authors of this article began to gain experience in this field with the development of a method to achieve precise focalization of a laser beam to be applied to an LBIC system (Laser Beam Induced Current) for the study of photovoltaic slides by analyzing line scans over sharp structures (Martin et al., 2004; Poce-Fatou et al., 2002).

Many of the methods described earlier were proposed before the mass use of computers with powerful calculation capacities and which were not fully developed in terms of the digital treatment of color images. These methods apply their algorithms on monochrome and polychrome images in which the only calculation variable is intensity or brightness and avoiding the treatment of color spaces.

A color space is a three-dimensional space used to represent any color in an organized way by choosing three coordinates that describe it (Wyszecki and Stiles, 1982). In computerized image treatment, the two most commonly used models are the red, green, and blue (RGB) and lightness, hue, and saturation (LHS) models. The former is used in most chromatic reproduction technology in which each color point is represented by the intensity of three chromatic transmitters emitting in red, green and blue (Foley, 1982). The intensity scale is usually divided into 256 sectors so the model is shaped like a Cartesian space with finite dimensions. In contrast, there is the family of LHS models, which essentially involve a conversion from Cartesian to cylindrical coordinates. This model is the one usually used for controlling the variable parameters of chromatic visualization devices as it adapts best to the way the human eye works (Levkowitz and Herman, 1993). The L coordinate is used in monochromatic representations, and thus, is the variable that is usually used for calculus algorithms. This variable does not correspond exactly with any of those used in the RGB model, but it is the G coordinate that carries most weight due to the human eye's greater sensitivity to the wavelength associated with that color.

For this reason, many algorithms developed do not cover all the possibilities as they do not take into consideration the individual influence of the RGB or LHS component of each pixel. This is extremely important since, depending on the image to be treated, it is possible to reach different results according to the chromatic coordinates of each pixel. Although the set of six chromatic variables is not a system of independent coordinates due to the subsets RGB and LHS being linked via mathematical expressions, it is possible for them to be considered quasi-independent due to the fact that the transformation relationship from one subset to another is not lineal and small variations from one of the primary colors of one of the subsets can greatly affect another from the other subset. However, it must be clarified that only a set of three of these six variables is truly independent. Thus, it is possible that an object with small variations in its chromaticity values ($H \sim$ cte.) has very different values from luminosity ($L \neq$ cte.), and saturation ($S \neq$ cte.) variables and any of the RGB coordinates. Therefore, the final results may depend on the chromatic coordinates used, and the user of the methodology must establish which color component it is most interesting to study for each set of images of the object, depending on its intrinsic color characteristics. Alternatively, it is possible to establish criteria for deciding which coordinates to use. In this article, we propose a method for making this decision based on the study of second variance.

MATERIALS AND METHODS

The methodology developed involves three steps: (a) obtaining a series of K digital images with a definition of $I \times J$ pixels, with each image at a different lens-object distance so that each one contains one or more focalized pixels of the object, (b) determining which set of three independent chromatic coordinates (RGBLHS) carries the greatest statistical weight in the three dimensional physical space $V(k,i,j)$ by maximization of the second variance of the chromatic coordinates in relation to the number of images and the number of pixels, and (c) determining which pixels (i,j) of each k image are considered to be focalized by calculating the variance in the surroundings of each weighted pixel.

To achieve optimal results in the process of extraction and accumulation of optically focused zones in each image it is important that the Δz separation between each pair of consecutive images is less than the optical depth of field, defined by the expression

$$\mathrm{DOF} = \frac{2\lambda}{\pi}\left(\frac{1}{2n\sin\theta}\right)^2, \qquad (1)$$

where DOF is the Depth of Field, n is the refractive index of the space in which the lens harvests photons, θ is the half angle of the observation cone and λ is the wavelength of the reference radiation, whose value is 550 nm (maximum sensitivity of the human eye and maximum solar irradiation). Our system has been automated so, using a MICOS SMC Pollux step-by-step motor attached to the micrometric displacement system of a Nikon Alphaphot YS2 microscope, it is possible to capture images along the Z axis with a theoretical resolution below 0.1 μm, which is a smaller interval than the depth of field of the objective lens being used. The images are taken using two systems: (a) an ISD camera (model uEye UI-1460-C) with a [1/2]″; / 3.2 Mp CMOS sensor and direct USB computer connection and (b) a Nikon Coolpix E995 with a 1/1.8″ and 3.3 Mp sensor and delayed USB computer connection. The different series of images were acquired with both cameras set to manual and under the same conditions regarding focal aperture, shutter speed, magnification, and light stability for images to be then compared correctly.

The positional coordinates (k,i,j) define the physical space in which we move, while the value of each of these coordinates provides the chromaticity value associated with it. Thus, the chromatic value of the pixel (i,j) in image k is defined as $V_{k,i,j}$ .This value can in turn be broken down into its three primary RGB components, indicating on a scale from 0 to 255 the amount red, green, and blue components that have to be used to reproduce the virtual chromaticity of the pixel. Within this framework, the $R_{k,i,j}$ variable defines the

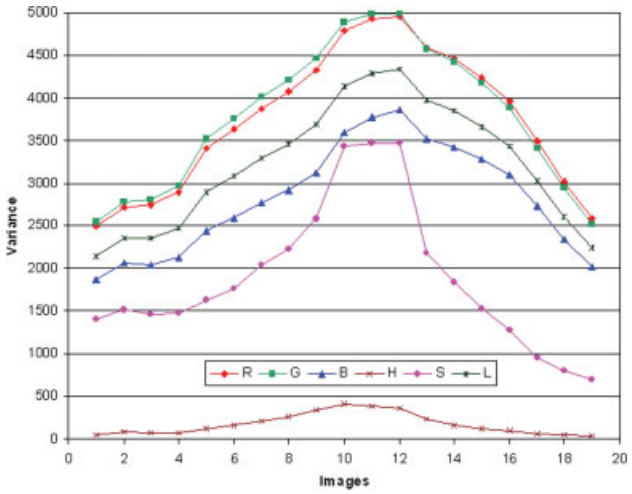

Fig. 1. Representation of variance of the RGB-LHS coordinates for a set of 19 images in which it is possible to see that the image with the best focalization is not the same for all the variables, but the tendency is very similar for any one of the chromatic coordinates. The best focalized image is number 12 for variables R, B, and L, while it is image 11 for coordinates G and S and image 10 for variable H. [Color figure can be viewed in the online issue, which is available at www.interscience.wiley.com.]

value of the red component (R) of the chromaticity in the spatial position defined by the indices *i, j,* and *k*. The variance of this component for each *k* image is calculated using the expression

$$\sigma^2(R) = \sum_{i=1}^{I}\sum_{j=1}^{J} \frac{\left(R_{i,j} - \sum_{i=1}^{I}\sum_{j=1}^{J}\frac{R_{i,j}}{I*J}\right)^2}{(I*J-1)}. \quad (2)$$

A similar situation can be reached if, instead of RGB components, LHS components are used. These components are defined for the chromatic space, which uses lightness, hue, and saturation as chromatic variables.

For a set of images, variance maximization is the methodology which is usually used to define which image is optimally focalized (Valdecasas et al., 2001). Applying this methodology to the set of images resulting from their breakdown into RGB and LHS form makes it possible to observe that the image with the best focalization is not always the same and depends on the color coordinate used. In Figure 1, it is possible to observe a graphic representation of the variance of a set of 19 images obtained for each of the chromatic coordinates. It can be appreciated that the image with the greatest variance value is not the same for all the chromatic variables. The best focalized image is number 12 for variables R, B, and L, while it is image 11 for coordinates G and S and image 10 for variable H. However, situations in which all the variances show a similar tendency do not always arise and it is possible to find cases in which there are much greater differences between the variances of one chromatic variable or another, as can be observed in Figure 2, where even the tendency of the curves is different for the six components.

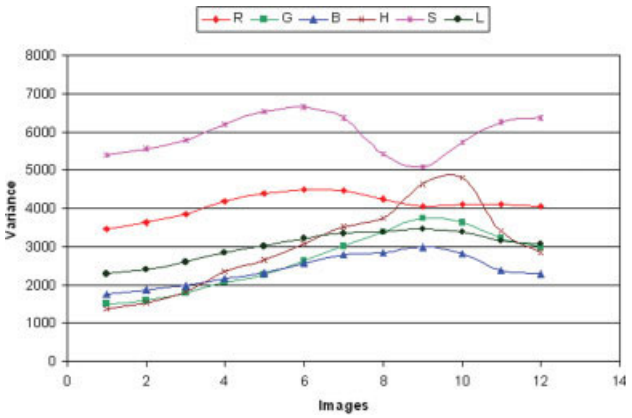

Fig. 2. Representation of variance of the RGB-LHS coordinates for a set of 12 images in which it is possible to see that the image with the best focalization is not the same for all the variables and that very different tendencies for some of the chromatic variables are observed. Thus, studying the variance of the different coordinates, it is not easy to determine which image has the best focalization overall. [Color figure can be viewed in the online issue, which is available at www.interscience.wiley.com.]

Thus, the most important chromatic variables when applying the algorithm to obtain the focalized segments of each image can be considered to be those with a greater variability in the variance or, equivalently, the second variance in relation to the number of pixels and the number of images, defined as

$$V''(R) = [\sigma^2(\sigma^2(R))] = \sum_{k=1}^{K} \frac{\left(\sigma_k^2(R) - \sum_{k=1}^{K}\frac{\sigma_k^2(R)}{K}\right)^2}{K-1}. \quad (3)$$

This is equivalent to calculating the variation of the chromatic variables in the K images, taking into account that the chromatic components showing a greater variation are those that will contribute most when applying the algorithm to obtain the segments of each image with the best focalization.

Algorithm for Obtaining the Sectors With the Best Focalization in Each Image

Starting with a set of *K* images, the algorithm that has been developed can be summarized in the following steps:

1. Each of the *K* images is broken down into its RGB and LHS chromatic components and for each of these the variance associated with the set of pixels of each image is calculated.
2. For each chromatic component, the variance associated with the set of data of the K images supplied in step 1 is calculated, defining the three chromatic components with the greatest statistical weight as those showing the highest variance value.
3. The numerical matrix $U_{k,i,j}$ is generated, where each component is calculated according to the formula

$$U_{k,i,j} = uR_{kij} + vG_{kij} + wB_{kij} + xL_{kij} + yH_{kij} + zS_{kij}, \quad (4)$$

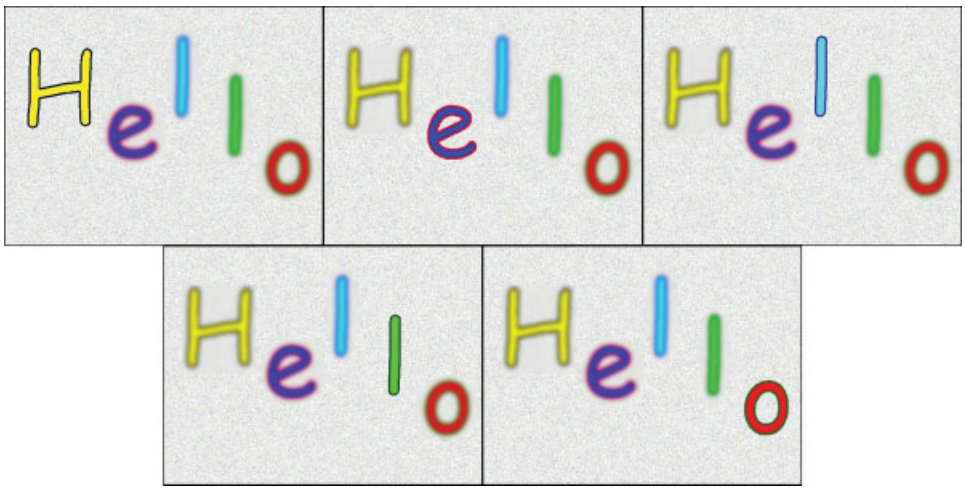

Fig. 3. Set of five design images in which only one of the letters is focalized in each one. These images were obtained from one initial image, parts of which were defocalized. [Color figure can be viewed in the online issue, which is available at www.interscience. wiley.com.]

where the coefficients $u \ldots z$ have values of 1 or 0, with 1 corresponding to the active chromatic components chosen in step 2, and 0 to the rest of the components.

4. The level of focalization associated with each point of the matrix $U_{k,i,j}$ is evaluated by measuring its variance in relation to the set of points defined for the k plane and formed by the existing points in s layers around the point being considered. This is done by extracting successive submatrixes centered on each $U_{k,i,j}$, element with the dimensions $2s+1$, (s = 1,2,3, ...) from the U matrix. The variance of each submatrix is calculated by applying Eq. (2), but substituting the average value with the value of the point being considered. As a way of emphasizing the differences between the layer of data nearest to each point and the rest of the layers, a weighting factor proportional to the inverse of the point's positional distance has been applied. Thus, a new matrix $W_{k,i,j}$ is obtained in which in each positional coordinate (k,i,j) the quadratic distances of each point (i,j) of each k layer appear in relation to the points of their surroundings. In this process the s layers of the outer pixels of each image must be sacrificed.
5. The vector W_k is extracted for each value of (i,j) and the position k(max) of the maximum value is established. The values of the chromaticity coordinates associated with the position $V_{k(\max),i,j}$ are taken as corresponding with the pixel with the best focalization for that spatial position among the K images analyzed.
6. If it is not possible to obtain a definite value or the doubt is greater than the threshold value, the basis for providing pixels will be to use those corresponding to the (i,j) coordinates of the images with the best overall focalization.

RESULTS

To assess the proposed working methodology and show the differences between applying the algorithm for different chromatic coordinates, two examples will be given. First, a set of five design images are studied. They are formed from one original image, parts of which were made to be out of focus. Second, a set of real images obtained with an optical microscope were used.

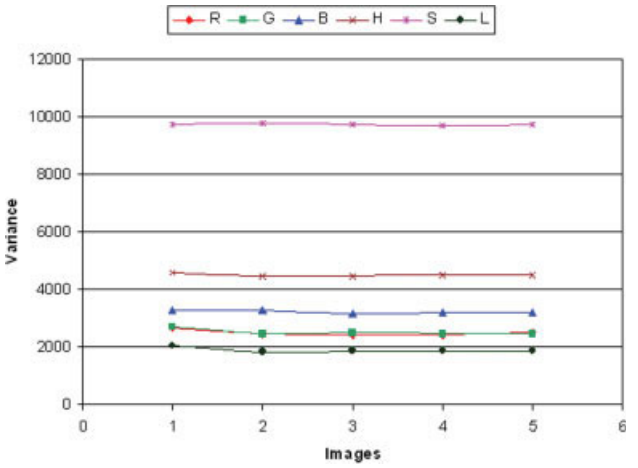

Fig. 4. Representation of the variance of the RGB-LHS coordinates for the set of images shown in Figure 3. The second variance of the six chromatic variables is calculated from these values, which are shown in Table 1. [Color figure can be viewed in the online issue, which is available at www.interscience.wiley.com.]

Design Images

An image was designed with the word HELLO with the following characteristics: (a) sharpness of the outlines, (b) high contrast between the edges of the letters, and (c) random chromatic noise in the space between the characters. The original image was submitted to a partial artificial defocalization using image processing software, creating a set of images that were partially out of focus in specific zones (Fig. 3). The focalization algorithm was applied to this set of images, analyzing the dependencies of the result obtained according to the chromatic components analyzed. Because they are synthetic images they all have similar chromatic parametres. Furthermore, the algorithm developed does not introduce false colors into the extended depth of field images it generates.

TABLE 1. Variance values for each of the six chromatic components

Chromatic coordinates	Second variance	Normalized second variance
R	12163	0.34
G	12148	0.34
B	2432	0.07
L	6053	0.17
H	1359	0.04
S	1442	0.04

As was detailed in the description of the procedure, the first step consists of calculating the variance for each of the chromatic components and for the five images. In Figure 4, we can observe the graphic representations of variance according to the number of the image for the chromatic variables RGB-LHS. Next, the second variance for the six variables was calculated, with the values obtained reflected in Table 1. From these values it is possible to conclude that the chromatic components that carry most weight when applying the algorithm are RGL, and the least are BHS.

Figure 5A shows the reconstructed image obtained by applying the algorithm to the RGL variables, while Figure 5B shows another obtained by applying the algorithm only to the L variable, which, as explained above, is the variable that is normally used by the algorithms found in the literature. Small differences can be observed between both images. In the image obtained with the RGL variables, the letter "e" (marked as 1) has a higher resolution around its whole outline than in the image obtained only with the L variable. Also, a higher resolution can be distinguished on the edges of all the letters, the most obvious case being in the letter "H" (marked as 2). That is, better focalization is achieved overall in the image obtained by applying the algorithm to the RGL variables. This is due to the fact that when the algorithm is applied exclusively to the L variable, the contribution of the RG variables is not considered. Looking at the data in Table 1, these variables show high second variance values and therefore carry more weight in the application of the algorithm. The difference that is observed would be even greater if the L variable carried less weight and so, in real cases, using only the Lightness variable (as the algorithms in the literature do) can lead to the best results not being achieved.

Figure 5C shows the image obtained when the algorithm is applied to the BHS variables, which carry the least weight in the calculation performed by the algorithm. If this image is compared with Figure 5A, the letters of the image appear with less definition around their outline. That is, the overall focalization of the image is worse.

In Figure 5D, the result of applying the algorithm on the six chromatic variables is shown. In this case, the resolution is better than when only the BHS variables (worse option) are used, but there is a loss of resolution in the letter "H" (marked as 2) when this is compared with the image obtained by applying the algorithm on the RGL variables (Fig. 5A).

A more objective comparison than simple visual appreciation is the calculation of variance of the set of pixels in the resulting image, with an image having better focalization if it maximizes the variance function (Valdecasas et al., 2001). Furthermore, the variance for each of the six chromatic variables is calculated since it has been shown that different results may be reached depending on the variables used. Variance was calculated for the images reconstructed when the algorithm is applied to the variables with the greatest statistical weight (RGL), the least weight (BHS), the L variable and all the chromatic variables, as well as the original image. Table 2 shows the data for the normalized difference image variance, which are weighted in relation to the normalized second order variance. The image with best focalization is the one where the sum of these values is lowest. This table shows that using the RGL coordinates as the basis for the calculation for the reconstruction of the image provides better results than the use of all the coordinates (RGBLSH) or only the L coordinate. It can also be seen that when we use the BHS variables (least weight) the image obtained shows better results for these variables but worse results for the other variables which have a greater statistical weight. This can be seen in the values shown in the last column of Table 2, corresponding to the sum of the data for all the coordinates. In this column we can appreciate that the best results are obtained using the three statistically most representative variables.

TABLE 2. Variance normalized difference values weighted with normalized second variance for each of the six chromatic components of the images obtained as a result of applying the algorithm to the five synthesized images

	Variance						
Image	R	G	B	L	H	S	SUM
Starting image	0.0	0.0	0.0	0.0	0.0	0.0	0.0
Result using RGL	17.4	10.8	3.5	0.4	2.2	0.1	34.4
Result using L	20.4	12.7	3.9	1.1	2.9	0.2	41.1
Result using BHS	27.0	20.4	3.4	6.2	2.2	0.1	59.3
Result using RGBHSL	19.2	11.8	3.9	0.8	2.7	0.2	38.5

Real Images

For the procedure to be carried out, 19 images were obtained which, together, show complete focalization of the entire observed field. Figure 6 shows some of the images captured, and it can be observed that there are focalized and unfocalized zones in each one. As we have previously indicated, all the images have been obtained under the same photographic conditions and the algorithm does not introduce false colors into the extended depth of field images. Therefore, the differences between each extended depth of field image obtained as a result of the application of mathematical algorithm are a direct consequence of the differences between the chromatic coordinate sets. The variance values obtained for the six chromatic variables are shown in Figure 1, while the values obtained for the second variance in relation to the number of pixels and the number of images is shown in Table 3. From these values, it can be deduced that the chromatic variables which carry the greatest weight when applying the algorithm will be RGS, although the B and L variables can make an important contribution. The value of the second variance obtained for the H variable is very low, so it contributes very little in our algorithm. Figure 7A shows the image, with extended depth of field, obtained by applying the algorithm only to the RGS variables, while Figure 7B shows the image obtained when the

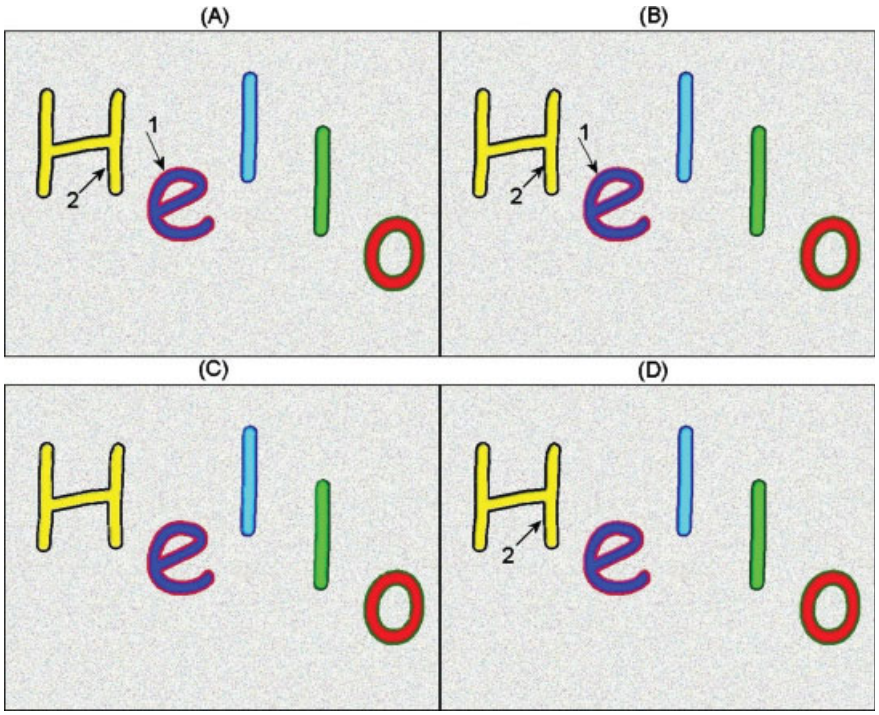

Fig. 5. Images obtained by applying the algorithm to the set of images shown in Figure 3. (**A**) using the RGL variables, which have the highest second variance values, as the basis for the calculation, (**B**) using only the L variable, (**C**) using the BHS variables, which have the lowest second variance values, as the basis for the calculation, and (**D**) using the six chromatic variables RGB-LHS. [Color figure can be viewed in the online issue, which is available at www.interscience.wiley.com.]

Fig. 6. Representative composition with some of the 19 images taken of a real sample (1 euro coin), using an optical microscope. All the images were captured using the same photographic conditions; resolution (640 × 480), focal distance (14 mm), aperture (f/3.3) and exposition (1/125s). [Color figure can be viewed in the online issue, which is available at www.interscience.wiley.com.]

algorithm is applied exclusively to the L variable, which is what the algorithms found in the literature do. Comparing both images, some differences can be observed in their resolution. It is possible to see that the shady areas of each image (marked as 1) show better focalization when the algorithm is applied to the RGS variables than with other variables.

On the other hand, Figure 8 shows the opposite case. This image shows the result of applying the algorithm

TABLE 3. Variance values for each of the six chromatic components

Chromatic coordinates	Second variance	Normalized second variance
R	683009	0.22
G	704088	0.23
B	416517	0.14
L	521701	0.17
H	15255	<0.01
S	715026	0.23

Fig. 7. Extended depth of field image obtained by applying the algorithm to the 19 real images of a coin obtained with a high magnification microscope. (**A**) using the RGL variables, which have the highest second variance values, as the basis for the calculation, and (**B**) using the L variable. [Color figure can be viewed in the online issue, which is available at www.interscience.wiley.com.]

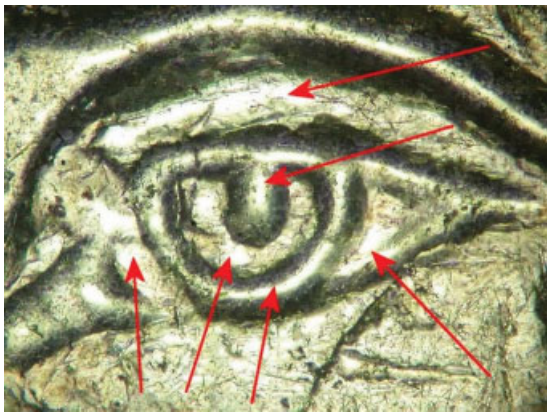

Fig. 8. Extended depth of field image obtained by applying the algorithm to the 19 real images of a coin obtained with a high magnification microscope using the H variable, which has the lowest second variance value, as the basis for the calculation. [Color figure can be viewed in the online issue, which is available at www.interscience.wiley.com.]

using the chromatic component H as the only calculation variable. This component, as was pointed out above, has an appreciably lower second variance value than the rest of the chromatic coordinates. If this image is compared with Figures 7A and 7B, they are seen to be very different. The image in Figure 8 has several zones that are not well defined, whereas in the other images these zones have better definition.

Table 4 shows values for the normalized difference variance, weighted with regard to the normalized second order variance, for the three images obtained by applying the algorithm based on the analysis of the RGS, L, and H variables. It can be observed that the variance value for the image obtained by applying the algorithm to the chromatic variables RGS shows better focalization than the image obtained by applying it to the L variable and appreciably better focalization than when only the H coordinate is used.

TABLE 4. Variance normalized difference values weighted with normalized-second variance for each of the six chromatic components of the images obtained as a result of applying the algorithm to 19 images taken of the sample under study using the different variables as the basis the calculation in each case

	Variance						
Image	R	G	B	L	H	S	SUM
Result using RGS	0.0	0.0	0.0	0.0	0.0	0.0	0.0
Result using L	4.9	5.1	2.6	3.7	0.0	7.1	23.4
Result using H	7.8	46.2	2.7	5.1	0.2	10.9	72.9

DISCUSSION

In this study, an algorithm to obtain images with extended focal depth of field from a set of images with only partial focalization was used. The methodology used makes it possible to show that the final resolution that can be obtained depends on the chromatic parameters used in the calculation, and their dependence on the intrinsic characteristics of the image, which are defined by the values of the chromatic coordinates R, G, B, L, S, and H. The use of the second variance of the chromatic coordinates in relation to the number of images and pixels makes it possible to visualize the dependence of the chromatic parameters with regard to the extended focalization methodology. Interdependencies are obtained that are an improvement on the approaches based on the exclusive use of the Lightness variable (L) as the basis for calculations.

The methodology is based on the calculation of the second variance of each of the six chromatic variables in all of the images acquired and the total number of pixels in these images. With this value it is possible to establish which chromatic variables carry the most weight when establishing which pixels are considered to be either in focus or having a value that does not depend on the displacement of the focal axis. It has been shown that the quality of the final image with extended depth of field varies depending on the variables used for the calculation and, therefore, the algorithms that are often used may produce flawed results because they do not use the most suitable variables. So, since a color space is three-dimensional, a suitable approach for deciding which chromatic coordinates to use when applying the algorithm to obtain the focalized zones of each image is to use the three chromatic variables with the highest second variance value.

The results obtained, for both the real images and the design images used as a control, endorse the proposed methodology. It is always possible to see more detail in the reconstruction when using suitable chromatic variables, which are defined as those carrying the greatest weight in the second variance. The use of

variables carrying less weight in the calculation of second variance as the basis for calculations can lead to results in which reconstructed images with extended depth of field show chromatic, and even geometric, distortions.

To confirm the quality of our system and algorithm we have compared the aforementioned examples with a methodology and algorithm developed by Forster et al. (2004) based on a complex-valued wavelet transform, which, like our algorithm, does not introduce false colors into the images obtained. To compare the images obtained with both methods, the variance of each image was calculated as, according to the literature, a higher value of variance implies better focalization (Valdecasas et al., 2001). With design images the improvement achieved was ~10%, while with the real images our results showed an improvement of 5%, according to the variance data calculated. This is due to the fact that it is not only the function used as the base of the algorithm that is important, but also the way that the function is applied to the images under study. The design images example is an extreme case, but it makes it possible to detect clearly the improvements that our algorithm provides.

REFERENCES

Amar N, Labbé A, Hamard P, Dupas B, Baudouin C. 2008. Filtering blebs and aqueous pathway: An inmunocytological and in vivo confocal microscopy study. Ophthalmology 115:1154–1161.

Burt PJ, Lolczynski RJ. 1993. Proceedings of the Forth International Conference on Computer Vision, Berlin, Germany, 173–182.

Castleman KR. 1996. Digital imaging processing. Englewood Cliffs, NJ: Prentice Hall.

Chen YC, Chen YC, Chiang AS. 2008. Template-driven segmentation of confocal microscopy images. Comput Methods Programs Biomed 89:925–936.

Foley JD. 1982. Fundamentals of Interactive Computer Graphics. Reading: Addison-Wesley.

Forster B, Van De Ville D, Berent J, Sage D, Unser M. 2004. Extended Depth-of-focus for multi-channel microscopy images: A complex wavelet approach. IEEE Int Symp Biomed Imaging: From Nano to Macro (ISBI'2004), Arlington, VA (USA), 660–663.

González RC, Woods RE. 1992. Digital imaging processing. Reading: Addison-Wesley.

Hashimoto S, Moon HR, Yoon KB. 2007. Optical microscopy study of zeolite-dye composite materials. Micropor Mesopor Mat 101:10–18.

Heisterkamp A, Baumgart J, Maxwell IZ, Ngezahayo A, Mazur E, Lubatschowski H. 2007. Fs-laser scissors for photobleaching, ablation in fixed samples and living samples, and studies of cell mechanics. Methods Cell Biol 82:293–307.

Iliev AI, Wouters FS. 2007. Application of simple photobleaching microscopy techniques for the determination of the balance between anterograde and retrograde axonal transport. J Neurosci Methods 161:39–46.

Itoh K, Hayashi A, Ichioka Y. 1989. Digitized optical microscopy with extended depth of field. App Opt 28:3487–3493.

Levkowitz H, Herman GT. 1993. GLHS: A generalized lightness, hue, and saturation color model. Graph Models Image Process 55:271–285.

Li H, Manjunath BS, Mitra SK. 1995. Multisensor image fusion using the wavelet transform. Graph Models Image Process 57:235–245.

Martín J, Fernández-Lorenzo C, Poce-Fatou JA, Alcántara R. 2004. A versatile computer-controlled high-resolution LBIC system. Prog Photovoltaics 12:283–295.

McCrickerd JT. 1971. Coherent processing and depth of focus of annular aperture imagery. App Opt 10:2226–2230.

Mironova EV, Evstratova AA, Antonov SM. 2007. A fluorescence vital assay for the recognition and quantification of excitotoxic cell death by necrosis and apoptosis using confocal microscopy on neurons in culture. J Neurosci Methods 163:1–8.

Nair MB, Babu SS, Varma HK, John A. 2008. A triphasic ceramic-coated porous hydroxyapatite for tissue engineering application. Acta Biomater 4:173–181.

Pieper RJ, Korpel A. 1983. Image processing for extended depth of field. App Opt 22:1449–1453.

Poce-Fatou JA, Martín J, Alcántara R, Fernández-Lorenzo C. 2002. A precision method for laser focusing on laser beam induced current experiments. Rev Sci Instrum 73:3895–3900.

Scalfi-Happ C, Jauss A, Ibach W, Hollricher O, Fulda S, Hauser C, Steiner R, Rück A. 2007. Confocal raman microscopy as a diagnostic tool for investigation of living neuroblastoma tumour cells. Med Laser Appl 22:157–164.

Scrimgeour J, Eriksson E, Goksor M. 2007. Laser surgery and optical trapping in a laser scanning microscope. Meth Cell Biol 82:629–646.

Snyder MA, Vlachos DG, Nikolakis V. 2007. Quantitative analysis of membrane morphology, microstructure, and polycrystallinity via laser scanning confocal microscopy: Application to NaX zeolite membranes. J Membrane Sci 290:1–18.

Sugimoto SA, Ichioka Y. 1985. Digital composition of images with increased depth of focus considering depth information. App Opt 24:2076–2080.

Valdecasas AG, Marshall D, Becerra JM, Terrero JJ. 2001. On the extended depth of focus algorithms for bright field microscopy. Micron 32:559–569.

Wickramasinghe SR, Carlson JO, Teske C, Hubbuch J, Ulbricht M. 2006. Characterizing solute binding to macroporous ion exchange membrane adsorbers using confocal laser scanning microscopy. J Membrane Sci 281:609–618.

Widjanarko T, Hardie RC. 2002. A post-processing technique for extended depth of focus in conventional optical microscopy. Opt Laser Technol 34:299–305.

Wyszecki G, Stiles WS. 1982. Color science: Concepts and methods, quantitative data and formulae. New York: Wiley.

Zhang G, Flach CR, Mendelsohn R. 2007. Tracking the dephosphorylation of resveratrol triphosphate in skin by confocal Raman microscopy. Biomaterials 28:4635–4642.